Photochemistry and Photobiology, 2018, 94: 1129–1137

A Comparative Study on the Photophysical and Photochemical Properties of Dyes in the Presence of Low Generation Amino-terminated Polyamidoamine Dendrimers†

Micaela E. Grassano, Marcela S. Altamirano, María P. Militello, Ernesto M. Arbeloa, Carlos M. Previtali* and Sonia G. Bertolotti*

Departamento de Química, Facultad de Ciencias Exactas Físico Químicas y Naturales, Universidad Nacional de Río Cuarto, Río Cuarto, Argentina

Received 5 July 2018, accepted 19 September 2018, DOI: 10.1111/php.13033

ABSTRACT

The photophysical and photochemical properties of the xanthene dyes mercurochrome (MCr) and eosin-Y (Eos); and the phenazine dye safranine-O (SF) are evaluated in the presence of amino-terminated polyamidoamine (PAMAM) dendrimers of low generations. The dendrimers produce a red shift in the UV-vis absorption spectra of the dyes, which increases with concentration and the size of the PAMAM molecule. The Stern–Volmer plots of fluorescence quenching for xanthenic dyes present a downward curvature. It is ascribed to a static mechanism involving a dye–dendrimer binding. A nonlinear fitting of the SV plots allows the calculation of the binding constants. For SF, the fluorescence is only slightly quenched by PAMAMs and the SV plots are linear. The binding constants are in the order K_{bind} (SF) $\ll$ K_{bind} (Eos) < K_{bind} (MCr). The difference must be due to important specific structural effects. A decrease in the triplet lifetime and an increase in the absorption of the semireduced form of the dyes are observed in the presence of dendrimers. While for the two xanthene dyes, the rate constants reach the diffusional limit for G2 and G3, for SF they are one order of magnitude lower. This is explained by a different quenching mechanism of the two types of dyes.

INTRODUCTION

It is well known that the optical properties of dyes hosted in constraint environments as direct and reverse micelles (1), liposome (2) or cyclodextrins (3) are very different from those in homogeneous media. Generally, such effects have been ascribed to the polarity sensed by the dye in the confined surroundings, which usually differs from that of the bulk solvent. This has led to use dyes as fluorescent probes for imaging and disease treatment (4) and for characterizing micro and nanoenvironments (5), which can be used as models of biological media. Another relevant application of confined dyes is as photoinitiating system of vinyl polymerization, in the presence of an electron donor. Recently, we synthesized latex nanoparticles of supercoiled polymers of high molecular weight by means of dyes hosted in reverse micelles (6,7).

In particular, the study and characterization of the optical properties of dyes bonded to, or hosted in dendrimers has become relevant. The interest lies on the potential applications of these dye–dendrimer systems to the field of chemical sensitizing (8), imaging (9), sensing (10), photoinduced polymerization (11) and photodynamic therapy (12) among others. Dendrimers and dendritic molecules are a particular class of confined environments, which behave as unimolecular micelles able to host small molecules inside (13,14). This unique feature depends mainly on the size of the dendrimer—so-called generation—because of the extent of branching determines the structure conformation that these molecules adopt in solution. For example, the first three generations (G0-G2) of polyamidoamine (PAMAM) and poly (propylene-amine) (POPAM) dendrimers have essentially open structures, whereas from G4 onwards a globular-like conformation is preferred. In general, an intermediate conformation between open and globular is assumed for G3 dendrimers (13).

Most reports on dye–dendrimer complexes refer to the xanthene family, which have been widely studied on the last decade. The concept of dendritic box for Rose Bengal encapsulation started a new subject of interest concerning this type of host/guest associations (15). Next works showed an efficient energy transfer from dansyl chromophores attached at the periphery of G4 POPAM dendrimers, to Eosin-Y (Eos) hosted inside (16,17). A series of subsequent reports accounted for detailed kinetic study on this light-harvesting system, by means of sophisticated time-resolved spectroscopies and molecular dynamic simulations (18–20). Following this topic, a comparative study between fluorescein, Eosin-Y and Rose Bengal hosted in POPAM dendrimers was also reported by the same authors (21). More recently, Dougherty *et al.* (22) isolated and characterized PAMAM-G5 dendrimers functionalized with two xanthene dyes at precise ratios, for imaging purposes. However, the encapsulation of some other dyes as phenol blue inside dendrimers was also quantified by spectroscopic techniques (23). Morgan *et al.* (24) found that a selective uptake occurred when quantitative solutions of PAMAM dendrimers, nile red and phenol blue were prepared.

In order to fully exploit the capabilities of such promissory dye–dendrimer complexes, a complete comprehension of their photophysical and photochemical properties is necessary. However, most of the research devoted to the light induced processes

*Corresponding authors' emails: cprevitali@exa.unrc.edu.ar (Carlos M. Previtali) and sbertolotti@exa.unrc.edu.ar (Sonia G. Bertolotti)
†This article is part of a Special Issue dedicated to Dr. Norman "Andi" García.

in these systems is circumscribed to singlet excited states of the dyes. It has not been given relevance to triplet states evaluation although the most of sensitizing reactions occur from them. It is also important to highlight that the moieties on the periphery and branches of dendrimers may promote the binding with dyes molecules even if the hosting is not possible. It is for this reason that to investigate the interactions between small size dendrimers and dyes is also pertinent to get insights about the driving mechanisms of host–guest complex formation with higher generations. Recently, we assessed the interactions between Eos and low generations of PAMAM dendrimers in aqueous solution and found that the extent of binding correlates with the dendrimer size (25). The photochemical dehalogenation of Eos promoted by electron transfer from PAMAM G0-G3 to the triplet state of the dye was also described (26). Such interesting results led us to expand our investigations toward the effect of higher PAMAM generations (G3-G5) on a series of xanthene dyes (27). A selective binding correlating with the hydrophilic–lipophilic balance of the dyes was observed. The triplet quantum yields of the dyes were strongly affected by the binding with dendrimers, and the high efficiencies of radical formation obtained with all analyzed dye–dendrimer couple suggested their potential application in the photopolymerization field.

On the other hand, although no binding is observed the dendrimer can still interacts with dyes in their vicinity. By quenching experiments we concluded that efficient electron transfer processes occurred from low generations of PAMAM and POPAM dendrimers to the excited states of Safranine-O in methanol solutions (28). To account for the effect of the peripheral groups of the dendrimers on the optical properties of dyes, the singlet and triplet excited states of Safranine-O were also evaluated in the presence of carboxyl-terminated PAMAM dendrimers in aqueous solution (29). Despite the scarce binding between this dye and PAMAM, high radical quantum yields were obtained from quenching of the triplet state of the dye by dendrimers.

Herein, we present a comparative study on the photophysical and photochemical properties of dyes from two different families in the presence of low generations of amino-terminated PAMAM dendrimers. The effect of PAMAM G0-G3 on the excited states of two anionic dyes, Eos and Mercurochrome (MCr) and a cationic phenazine one, Safranine-O (SF) in alkaline aqueous solution, was evaluated by absorption and fluorescence spectroscopies and laser flash photolysis.

MATERIALS AND METHODS

The dyes Eos, MCr and SF were from Aldrich and used without further purification. Amino-terminated PAMAM dendrimers of generations 0–3 (G0–G3) were obtained from Aldrich as a 20% methanol solution and were used as received. Aqueous solutions were prepared with HPLC-grade water (Sintorgan), and the pH was adjusted with a borate buffer.

Absorption spectra were recorded on a Hewlett Packard 6453E diode array spectrophotometer. Fluorescence determinations spectra were carried out with a Horiba Jobin Yvon FluoroMax-4 spectrofluorometer. A 1-cm path length quartz cell was used in all spectroscopic assays. The concentrations of xanthene dyes in the solutions were calculated from the respective molar extinction coefficients. Throughout all experiments, the addition of dendrimers was performed using microsyringes under constant stirring, such that the methanol contents in the dyes solutions were <5%. All data were properly corrected by dilution effects. The measurements were performed at least in duplicate.

Transient absorption spectra and triplet quenching were determined by laser flash photolysis. A Spectron SL400 Nd:YAG laser generating λ = 532 nm laser pulses (20 mJ per pulse, ca. 18 ns full-width at half-maximum) was the excitation source. The experiments were performed in right-angle geometry. The laser beam was defocused to cover the entire path length (10 mm) of the analyzing beam from a 150 W Xe lamp. The detection system comprised a PTI monochromator coupled to a Hamamatsu R666 PM tube. The signals were acquired and averaged by means of a digital oscilloscope (DSO6012A Agilent Technologies) and then transferred to a computer. All determinations were performed at (20 $\pm$ 1) °C, and the solutions were deoxygenated by bubbling with solvent-saturated, high-purity argon.

RESULTS AND DISCUSSION

Absorption, fluorescence and binding

Mercurochrome. Absorption spectra of MCr in aqueous buffer at pH 9 in the presence of amino-terminated PAMAM dendrimers are shown in Figs. 1 and 2, and the spectral characteristics are summarized in Table 1.

The dendrimers produce a red shift in the spectra. This red shift increases with the size of the PAMAM molecules and with its concentration. It may be estimated that the absorption maximum of the dye fully incorporated to the dendrimer is at 516 nm based on the extrapolation of the recorded spectral data. The changes in absorption maximum may be explained by a dye–dendrimer association (25–27). The inset in Fig. 1 shows the effect of the PAMAM G1 concentration on the dye absorbance at 528 nm. Similar plots were obtained for the other dendrimers (see Figure S1).

The absorbance changes at a given wavelength can be fitted with an association model, assuming a 1:1 stoichiometry for the MCr/dendrimer complex (*MCrPm*). A binding constant may be written as follows:

$$K_{\text{bind}} = \frac{[MCrPm]}{[\text{MCr}]\,[Pm_f]} \tag{1}$$

This assumption is reasonable because the dendrimer concentration was at least 200-fold greater than that of the dye for all generations used. Also, equivalent and independent sites were assumed. The same assumptions have been made by other

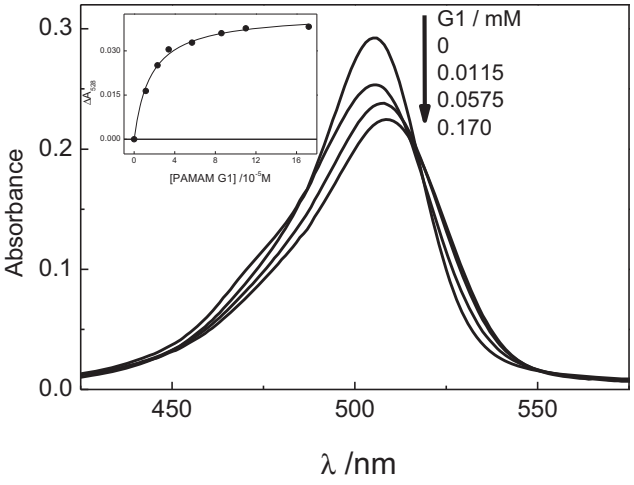

Figure 1. Absorption spectra of MCr as a function of polyamidoamine (PAMAM) G1 concentration. Inset: Absorption difference at 528 nm, the solid line is the fitting to Eq. (3). MCr concentration ca. 4×10^{-6} M.

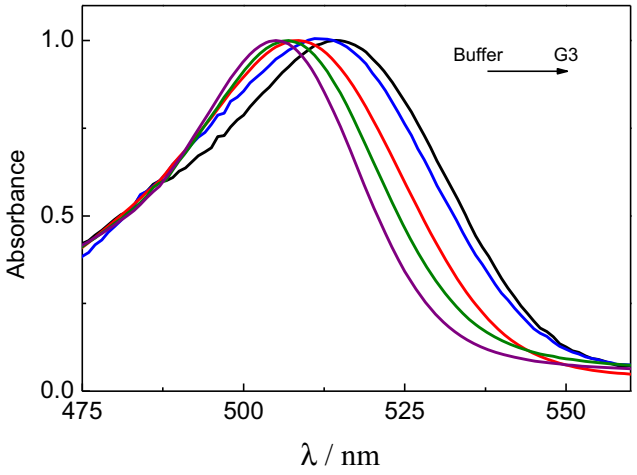

Figure 2. Normalized absorption spectrum of MCr in the presence of different generation of polyamidoamine (PAMAM) dendrimers in buffer pH 9. (—) MCr in buffer. (—) G3 (9.7×10^{-5}M), (—) G2 (5.3×10^{-5}M), (—) G1 (1.15×10^{-4}M) and (—) G0 (2.44×10^{-4}M).

Table 1. Absorption maximum of mercurochrome in the presence of polyamidoamine dendrimers in water at pH 9.

	Absorption (nm)
Buffer pH9	505
G0 2.4×10^{-4} M	506
G1 1.7×10^{-4} M	509
G2 5.3×10^{-5} M	512
G3 1.4×10^{-4} M	515

authors to determine K_{bind} values of PAMAM with several drugs (30,31).

When PAMAM is added the observed absorbance in the 450–600 nm range may be written as (25)

$$A = A_{free} + A_{bind} = \varepsilon_f[\mathrm{MCr}_f] + \varepsilon_{bind}[MCrPm], \quad (2)$$

since PAMAM dendrimers do not absorb in the visible region. In Eq. (2) ε_f and ε_{bind} stand for molar extinction coefficients of free and associated dye, respectively, at the observation wavelength. Considering Eqs. (1) and (2), the absorbance at a given wavelength is given by

$$A - Ao = \frac{[MCr_o]K_{bind}\ \Delta\varepsilon\ [Pm]}{1 + K_{bind}\ [Pm]}, \quad (3)$$

here $[MCr_o]$ is the analytical dye concentration, Ao is the absorbance in the absence of dendrimer; and $\Delta\varepsilon = \varepsilon_{bind} - \varepsilon_f$. In this equation, $[Pm]$ represents the total dendrimer concentration. This approximation is reasonable because of the excess of dendrimer used. From plots of $A\text{-}A_0$ at a given wavelength *vs* PAMAM concentration by a nonlinear fit analysis of Eq. (3) K_{bind} can be obtained. The binding constants obtained in this way are shown in Table 2. Although some differences in the values obtained by the different experimental techniques is apparent, they follow the same trend and are of similar order of magnitude reflecting the effect of the dendrimer size on the binding. It is well known that different experimental procedures and even differences in the treatment of the data lead to differences in the values of binding constants (32,33).

Eosin and safranine. The absorption maximum of Eos is shifted from 517 in pure alkaline water to 526 nm in the presence of PAMAM-G3, while there is a smaller red shift in the fluorescence emission (25). The absorption spectrum of SF in the presence of PAMAM presents a very small red shift. Thus, for G2 2.6 mM, the red shift is ca. 3 nm, while for the similar concentration of the dendrimer, Eos absorption shifts by 6 nm and MCr by 8 nm. As an example, the effect of PAMAM G3 on the absorption spectrum of SF is presented in Fig. 3. Due to the very small changes in the absorption spectra, the binding constants of SF were determined by fluorescence measurements.

Fluorescence in the presence of PAMAM

Xanthene dyes. The fluorescence quenching of eosin by PAMAM dendrimers was discussed in our previous publication (25). From an analysis of the data, Eos-PAMAM binding constants were determined and they are shown in Table 2. The other xanthene dye investigated, MCr, fluoresces in buffer solution pH 9 with $\lambda_{max} = 530$ nm. The emission maxima in the presence of PAMAMs are unchanged regardless of the dendrimer size or its concentration. However, an important quenching effect is observed in the presence of the dendrimers. The quenching may be explained by a static mechanism since the fluorescence lifetime (2 ns in water pH 8 ref. 34) is not affected by the PAMAMs even at the highest concentration investigated (1 mM), similarly to what was observed for Eos (25). The Stern–Volmer plots present a downward curvature, which can be ascribed to the residual emission of the dye bound to the dendrimer (Fig. 4).

The fraction of MCr molecules that are bound to the dendrimer α can also be expressed in terms of the fluorescence intensity as follows

$$\alpha = \frac{Fo - F}{Fo - F^*}, \quad (4)$$

where Fo and F stand for fluorescence intensity in the absence and presence of dendrimer. F^* is the residual emission when hypothetically all the dye would be bonded to dendrimer. In terms of the binding constant K_{bind}, the dependence of the fluorescence intensity with the PAMAM concentration can be written as follows:

$$F^0 - F = \frac{K_{bind}\ [Pm](F^0 - F^*)}{1 + K_{bind}\ [Pm]}. \quad (5)$$

Equation (5) may be rearranged to a form similar to a Stern–Vomer plot, *Fo/F* (29).

$$\frac{F^0}{F} = \frac{1 + K_{bind}\ [Pm]}{1 + (F^*/F^0)K_{bind}\ [Pm]} \quad (6)$$

In the absence of residual emission ($F^* = 0$), Eq. (6) reduces to Stern–Volmer equation with $K_{bind} \equiv K_{SV}$. A nonlinear fitting of the SV plots allows the calculation of binding constants for the system MCr-PAMAM, and they are collected also in Table 2. Although differing in values, they are of the same order of magnitude than those determined by the absorption spectra. In

Table 2. Binding constants and residual fluorescence from absorption spectra and fluorescence quenching at pH 9.

Polyamidoamine	Eos-Y[a]		MCr			SF
	K_{bind}/M^{-1}	F^*/Fo	K_{bind}/M^{-1}	F^*/Fo	K_{bind}/M^{-1} (absorption data)	K_{bind}/M^{-1}
G0	95	0.53	13 200 ± 2000	0.54	30 000 ± 4000	5.4 ± 2
G1	1200	0.41	30 000 ± 4000	0.33	62 000 ± 5000	17 ± 5
G2	5600	0.33	120 000 ± 20 000	0.29	101 000 ± 11 000	42 ± 8
G3	14 500	0.19	260 000 ± 30 000	0.08	150 000 ± 30 000	142 ± 20

[a]From ref. 25.

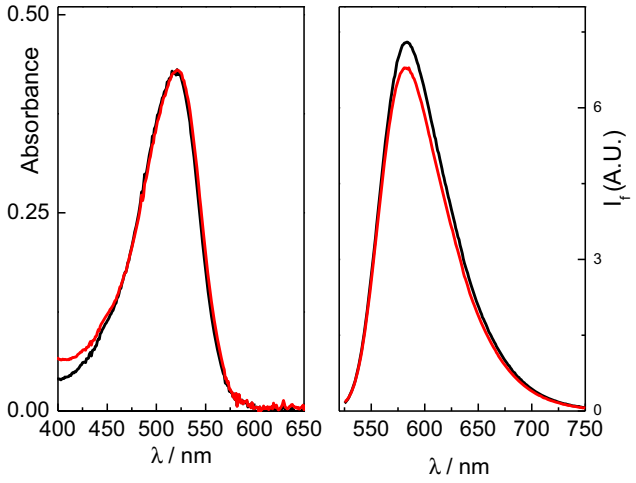

Figure 3. Absorption and fluorescence spectra of SF in the absence (—) and the presence (—) of polyamidoamine (PAMAM) G3.

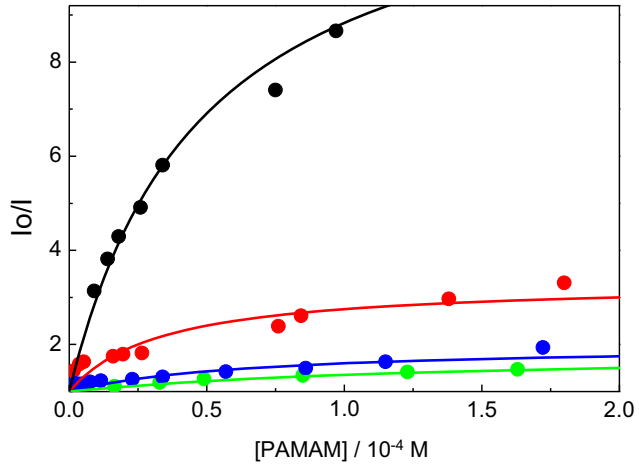

Figure 4. Stern–Volmer plots for the fluorescence quenching of MCr by polyamidoamine (PAMAM) dendrimers. (—) G3. (—) G0.

any case, they are very much higher than those for Eos. Also in Table 2 is included the fractional residual emission, (F^*/Fo) obtained from the nonlinear fitting of the absorbance *vs* PAMAM concentration (see Figure S1). It can be seen that the residual emission gradually decreases with the size of the PAMAMs. This is only discernible in the cases of Eos and MCr, while for SF, the low quenching efficiency results in linear plots that preclude the evaluation of this quantity. This was already observed for the case of Eos where a possible explanation is presented. This is another example of the selectivity of PAMAMs dendrimers for the binding of molecules consisting of the same structural skeleton but with different pendant groups (27).

Safranine fluorescence quenching by PAMAMs. There is a small blue shift in the SF fluorescence spectrum caused by the PAMAMs; thus, for G2 0.039 mM, it is ca. 2 nm. In part it may be attributed to the small percentage of MeOH added with the dendrimer concentrated stock solution. Nevertheless, it is known that the fluorescence emission of SF experiences a blue shift when the solvent polarity decreases (35). The fluorescence is only slightly quenched by PAMAMs. Stern–Volmer plots are shown in Fig. 5.

SF fluorescence lifetime in aqueous medium is 1.1 ns (35). Therefore, at the low molar concentrations employed the possibility of dynamic collisional quenching may be ruled out. Since SV plots are linear, the slope may be assigned to the dye–dendrimer binding constant. The values are shown in Table 2. It is noticeable the very much smaller values of these constants when compared to those of the xanthene dyes eosin and mercurochrome. This could be explained by the positive charge of the dye and the positive surface of the dendrimers structure; since at pH 9 still 30–40% of the terminal amino groups are protonated (36,37).

However, when similar experiments were carried out with carboxyl-terminated PAMAM dendrimers, the values of the binding constants although much higher than those for full generation PAMAMs of similar size are very much lower than those of xanthene dyes (29). Therefore, the effect must be ascribed to an important specific structural effect that renders a lower affinity of the substituted phenazine ring of Sf for the aminoamide chains of the dendrimers. The structural selectivity of low generation PAMAMs dendrimers toward small organic molecules is of interest in relation to the use of PAMAMs as potentials agents in drug delivery systems.

Triplet state

Mercurochrome. The effect of dendrimers on the excited triplet state of the dyes was investigated by means of laser flash photolysis. At short times, after the laser pulse at 532 nm, the difference transient absorption spectrum of MCr in buffer pH 9 presents two maxima at 370 and 555 nm that can be ascribed to the T-T transition. The spectrum is similar to those reported for other xanthene dyes (34). After the triplet decay, an absorption in the region 300–500-nm remains which can be ascribed to the simultaneous absorption of the semireduced and semioxidized forms of the dye. This can be explained in terms of the self-quenching reaction of the triplet state by ground state molecules. At pH > 7 MCr exists mainly as a dication (38,39) and the process may be written as follows:

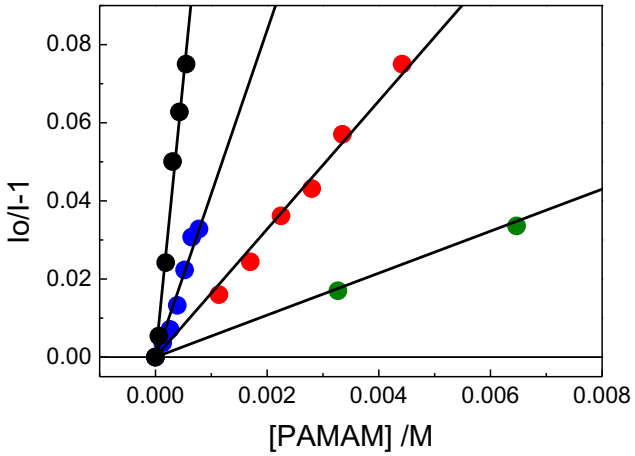

Figure 5. Stern–Volmer plots for the fluorescence quenching of SF by polyamidoamine (PAMAM) dendrimers at pH 9. (—) G3, (—) G1, (—) Go and (—) G2.

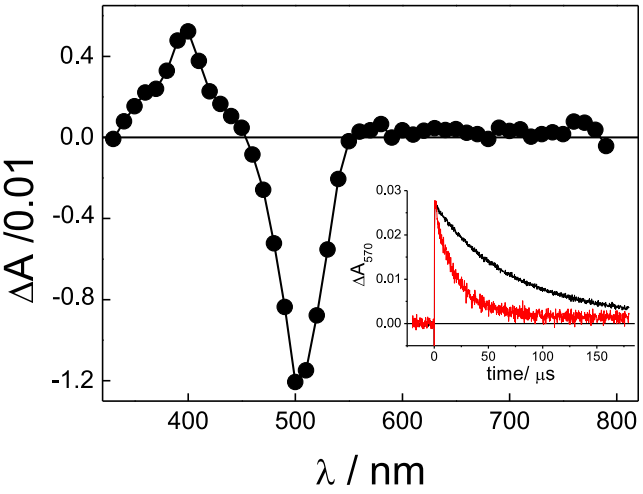

Figure 6. Transient absorption spectrum of MCr in buffer pH 9 in the presence of polyamidoamine (PAMAM) G2 2×10^{-5} M taken at 150 μs after the laser pulse. Inset: Decay at 570 nm in the absence (—) and the presence (—) of PAMAM G2 2×10^{-5} M.

$$^3MCr^{=} + MCr^{=} \rightarrow MCr^{3-\cdot} + MCr^{-\cdot}$$

The semireduced form absorbs ca. 400 nm with λ_{max} depending on the pH and polarity of the medium, while the semioxidized form is expected to absorb around 440 nm, by analogy with other xanthene dyes (40,41). This is confirmed by the transient spectra in the presence of electron donors and acceptors resulting by the electron transfer quenching of the triplet state.

In the presence of PAMAM, the initial transient absorption spectrum correspond to the triplet state, while the long-lived spectrum, after the triplet decay, presents only one band at 400 nm that may be assigned to the semireduced radical of MCr (42), Fig. 6.

In the presence of the dendrimers, the triplet decays monoexponentially. Triplet quenching rate constants (k_q) were determined by triplet lifetime (measured by the T-T absorption at 570 nm) as a function of quencher concentrations according to:

$$\tau^{-1} = \tau_0^{-1} + k_q[Pm] \quad (7)$$

where τ and τ_o are the triplet lifetime, in the presence and the absence of the dendrimer, respectively, and [*Pm*] is the analytical concentration of the dendrimer. Plots according to Eq. (7) are shown in Fig. 7, and the rate constants obtained from the slopes are shown in Table 3. At the concentrations employed in the triplet quenching experiments, most of the dye molecules are free, and the quenching process may be understood by a dynamical mechanism. No appreciable singlet quenching takes place at these concentrations.

Safranine. The T-T absorption of SF presents maxima at 800 and 710 nm in aqueous media. The triplet is quenching by PAMAMs, and the plots of the decay lifetime at pH 8, measured at 800 nm, are shown in Fig. 8. In this case, measurements were carried out at pH 8 in order to make sure that the triplet state corresponds to the monocationic form of the dye (43,44). The plots show a noticeable downward curvature with the exception of G0, which is linear. This behavior is similar to that observed for the quenching of triplet state of the dye in methanolic solution (28). The phenomenon was explained in terms of proton transfer equilibrium prior to the electron transfer final process (44).

The initial slope of these plots can be taken as an approximation to the rate constant in the quenching mechanism. They are also included in Table 3. From an analysis of the data in Table 3, it is observed that, with the exception of the case SF-G3, the rate constants increase with the size of the PAMAM dendrimer. However, an important difference in the values is apparent. While for the two xanthene dyes, the rate constants reach the diffusion limit for G2 and G3, for safranine they are one order of magnitude lower. Other difference is that for MCr and eosin the rate constant is two orders of magnitude higher than for aliphatic amines (42), whereas for safranine the values are of the same order of magnitude. All this reflects the different quenching mechanism of the two types of dyes. An electron transfer process from the amino groups of the dendrimers to the triplet state of the dye is operative in the case of both xanthene dyes. On the other hand, the quenching of SF involves an initial

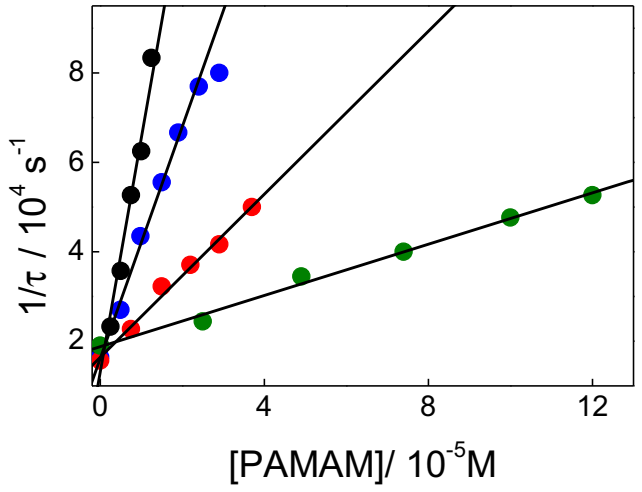

Figure 7. $1/\tau$ *vs* [PAMAM] for the triplet quenching of MCr with each dendrimer generation at pH 9. Black G2, red G3, blue G1 and green G0.

Table 3. Triplet quenching rate constants by polyamidoamine (PAMAM) dendrimers. Initial slopes of $1/\tau$ *vs* [PAMAM] in units of $M^{-1}s^{-1}$.

	SF	Eos-Y	MCr
G0	5.4×10^7	6.8×10^8	2.9×10^8
G1	8.7×10^7	1.6×10^9	9.1×10^8
G2	2.8×10^8	3.7×10^9	2.6×10^9
G3	1.9×10^8	4.7×10^9	5.0×10^9

Estimated error in rate constants is ±20%.

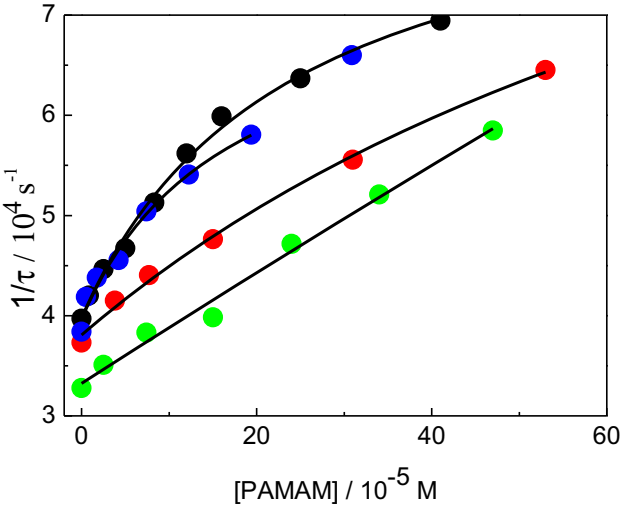

Figure 8. $1/\tau$ *vs* [PAMAM] for the triplet quenching of SF with each dendrimer generation at pH 8. (—) G3, (—) G1, (—) Go and (—) G2.

fast proton transfer step followed by a slower electron transfer reaction. The same considerations as before, regarding possible singlet quenching in the determination of triplet quenching rate constants, apply in the case of SF.

Long-lived transient absorptions

The quenching mechanism of triplet Eos was discussed in ref. 26. An initial electron transfer step produces the semireduced form of the dye, and this is followed by a debromination reaction of the intermediates. Similarly, for the MCr, the triplet quenching is explained by an electron transfer reaction, to yield the semireduced radical form of the dye.

Radical quantum yields for the quenching reaction of triplet MCr by PAMAM dendrimers were obtained from Eq. (8)

$$\Phi_R = \frac{\Delta A_R \varepsilon_T}{\Delta A_T \varepsilon_R} \frac{\Phi_T}{f} \tag{8}$$

Here ΔA_R is the long time absorption remaining after the triplet decay in the presence of the dendrimer measured at 390 nm, ΔA_T is the prompt T-T transient absorption measured at 570 nm immediately after the laser pulse, ε_R and ε_T are the respective molar absorption coefficients and Φ_T is the triplet quantum yield in the presence of the dendrimer. The T-T extinction coefficient at 570 nm, ε_T equals 6300 l mol^{-1} cm^{-1}, ε_R = 31 000 l mol^{-1} cm^{-1} and Φ_T = 0.40 from ref. 42. The fraction of triplets intercepted by the quencher Q is given by

$$f = \frac{k_q[Q]}{k_o + k_q[Q]} \tag{9}$$

In Fig. 9, an example of the measurements by laser flash photolysis can be seen. The quantum yields determined in this way are presented in Table 4. The radical yields are lower than those for the triplet quenching by aliphatic amines but of the same order than those for the quenching of Eos triplet by PAMAM dendrimers (26). For MCr, the yield is practically independent of the dendrimer size, as diverse for Eos where the quantum yield was higher for G0 than for G3. This may be related to the higher affinity of MCr for the dendrimers of higher generation. Several factors can account for the lower quantum yields in the triplet quenching by dendrimers compared to those with small aliphatic amines, and the most significant is a higher recombination of the radicals initially formed, due to an inhibition of the escape from the dendrimer domain. A similar phenomenon was observed in the triplet quenching of Eos by aliphatic amines when the reactants were confined in the water pool of reverse micelles (45). A fast recombination reaction was offer as an explanation of the very low radical yield.

Transient spectra of SF in the presence of PAMAM G0 are shown in Fig. 10. After the typical T-T absorption with maxima at 800 and 710 nm, the remaining spectrum presents a broad band at 600–650 nm and a second band at 420 nm. As can be seen in the inset, the long time spectrum is coincident with that in basic medium and can be assigned to the deprotonated triplet state of the dye. This is a confirmation of the quenching mechanism discussed above.

A similar effect was found with dendrimers of higher generation. In Fig. 11, the transient spectra in the presence of PAMAM G2 1 mM and that in basic media are compared. The similarity of the spectra in the region of 570–770 nm confirms that the initial quenching process in the presence of PAMAM is proton transfer from the triplet sate to yield the deprotonated excited triplet of the dye.

After the initial proton transfer process, a slower electron transfer reaction from the dendrimer to the deprotonated triplet takes place. This is illustrated in Fig. 12 where the absorption

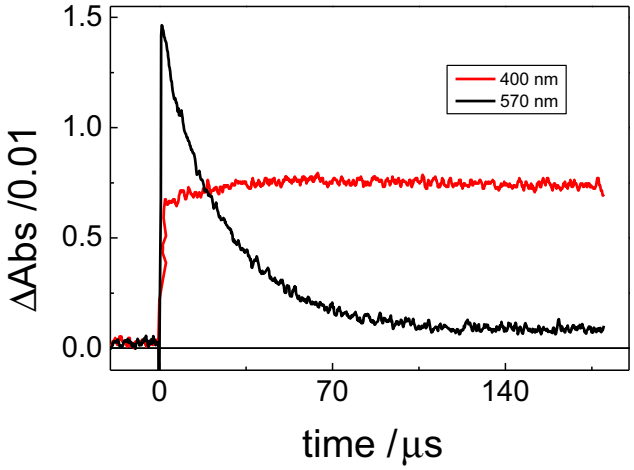

Figure 9. Absorption time profile at 570 and 400 nm of MCr in the presence of polyamidoamine (PAMAM) G3 5.5×10^{-6} M.

Table 4. Radical quantum yield in the triplet quenching of MCr by polyamidoamine (PAMAM) dendrimers.

	f	[PAMAM]/M	ΔA_T	ΔA_R	Φ_R
Buffer pH 9			0.021	0.01	0.038
G0	0.77	1.6E-4	0.004	0.003	0.079
G1	0.55	2.2E-5	0.0085	0.0045	0.072
G2	0.87	1.9E-5	0.009	0.0052	0.053
G3	0.50	5.5E-6	0.0145	0.007	0.078
TEOA[a]					0.23

Estimated error in radical quantum yields is ±20%. [a]At 20 mM TEOA from ref. 40.

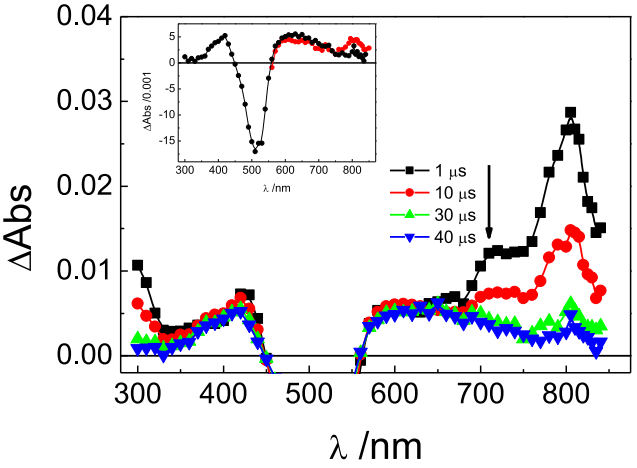

Figure 10. Transient absorption spectra of SF in the presence of polyamidoamine (PAMAM) G0 5×10^{-4} M. Inset: Absorption spectrum at 40 μs (—) and in water with added NaOH 10^{-4} M at 20 μs after the laser flash (—).

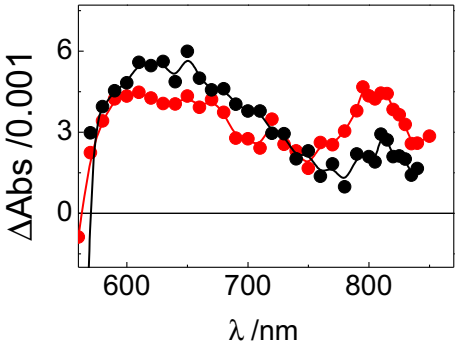

Figure 11. Transient absorption spectra of SF in the presence of polyamidoamine (PAMAM) G2 1 mM (—) and NaOH 0.1 mM (—).

profiles of transient species of SF after the laser pulse at 532 nm in the presence of PAMAM G2 1 mM in buffer pH 8 are shown.

It can be seen that after the triplet decay at 800 nm, the long time absorption in the zone of 400 nm keeps growing in the time window explored. Since the semireduced form of the dye is known to absorb in the region around 400 nm (46), the growing at this wavelength is an evidence of a second slow process, the electron transfer to the deprotonated triplet, taking place after the initial triplet decay.

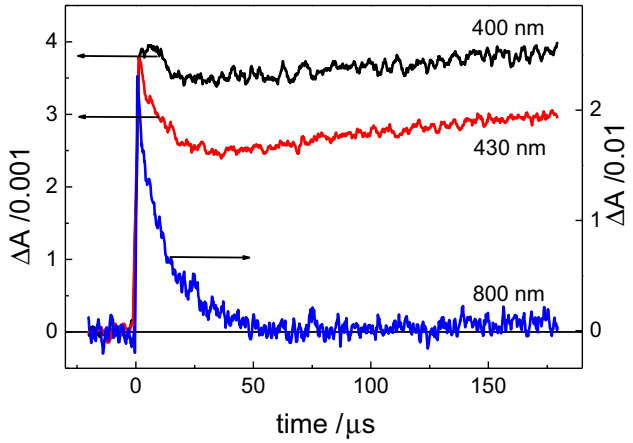

Figure 12. Decay profiles of safranine in the presence of polyamidoamine (PAMAM) G2 1 mM at different wavelengths. 800 nm (—), 430 nm (—) and 400 nm (—).

CONCLUSIONS

Polyamidoamine dendrimers produce a red shift in the UV-vis absorption spectra of the dyes investigated. This red shift increases with the size of the PAMAM molecules and with its concentration. An important fluorescence quenching effect of PAMAMs is observed for xanthene dyes. A nonlinear fitting of the SV plots allows the calculation of binding constants. These are higher for the system MCr-PAMAM, than for Eos-PAMAM. On the other hand, SF fluorescence is only slightly quenched by PAMAMs. Stern–Volmer plots are linear and from the slopes the dye–dendrimer binding constants were obtained. These constants are several orders of magnitude lower than those of xanthene dyes.

Triplet–triplet absorption spectra of the dyes are recorded by laser flash photolysis, and a decrease in the triplet lifetimes is observed in the presence of dendrimers. At the same time, an increase in the absorption of the semireduced form of the dyes is observed. Rate constants for triplet quenching (^3k_q) are obtained, and the rate constants reach the diffusion limit for G2 and G3 for Eos and MCR. The rate constants are two orders of magnitude higher than for aliphatic amines. The results are explained by a very efficient electron transfer process from PAMAM to xanthene dyes for all of the dye/dendrimer couples that are evaluated.

For SF, the triplet quenching rate constants are one order of magnitude lower that the diffusion limit and the values are of the same order of magnitude than for aliphatic amines. The quenching mechanism was explained in terms of the reversible formation of an intermediate complex in the excited state. The results were interpreted in terms of a reversible proton transfer quenching. This was further confirmed by the transient absorption spectra obtained by laser flash photolysis. The transient absorption immediately after the triplet state quenching could be assigned to the unprotonated form of the dye. At later times, the spectrum matches the semireduced form of the dye. The overall process corresponds to a one-electron reduction in the dye mediated by the deprotonated triplet state.

Acknowledgements—This work was supported by CONICET (PIP: 2015 - 11220150100687CO), and the Universidad Nacional de Río Cuarto.

M.P.M. thank CONICET for a postgraduate studentship. S.G.B., E.M.A. and C. M.P. are research members of CONICET, Argentina.

SUPPORTING INFORMATION

Additional supporting information may be found online in the Supporting Information section at the end of the article:

Figure S1. Absorption difference at specified wavelength as a function of concentration for the different PAMAM, the solid line is the fitting to Eq. (3) (MCr concentration ca. 4×10^{-6} M).

REFERENCES

1. Porcal, G. V., C. M. Previtali and S. G. Bertolotti (2009) Photophysics of the phenoxazine dyes resazurin and resorufin in direct and reverse micelles. *Dyes Pigm.* **80**, 206–211.
2. Bose, D., D. Ghosh, P. Das, A. Girigoswami, D. Sarkar and N. Chattopadhyay (2010) Binding of a cationic phenazinium dye in anionic liposomal membrane: A spectacular modification in the photophysics. *Chem. Phys. Lipids* **163**, 94–101.
3. Fini, P., M. Castagnolo, L. Catucci, P. Cosma and A. Agostiano (2004) Inclusion complexes of Rose Bengal and cyclodextrins. *Thermochim. Acta* **418**, 33–38.
4. Miksa, B., M. Sierant, E. Skorupska, A. Michalski, S. Kazmierski, U. Steinke, A. Rozanski and P. Uznanski (2017) Chlorambucil labelled with the phenosafranin scaffold as a new chemotherapeutic for imaging and cancer treatment. *Colloids Surf. B Biointerfaces* **159**, 820–828.
5. Pereira, P. C.d. S., P. F.d. A. Costa, D. S. Pellosi, I. R. Calori, B. H. Vilsinski, B. M. Estevão, N. Hioka and W. Caetano (2017) Photophysical properties and interaction studies of Rose Bengal derivatives with biomimetic systems based in micellar aqueous solutions. *J. Mol. Liq.* **230**, 674–685.
6. Porcal, G. V., E. M. Arbeloa, C. A. Chesta, S. G. Bertolotti and C. M. Previtali (2013) Visible light photopolymerization in BHDC reverse micelles. Laser flash photolysis study of the photoinitiating mechanism. *J. Photochem. Photobiol. A Chem.* **257**, 60–65.
7. Arbeloa, E. M., G. V. Porcal, S. G. Bertolotti and C. M. Previtali (2015) Synthesis and characterization of latex nanoparticles using a visible-light photoinitiating system in reverse micelles. *Colloid Polym. Sci.* **293**, 625–632.
8. Alamry, K. A., N. I. Georgiev, S. A. El-Daly, L. A. Taib and V. B. Bojinov (2015) A ratiometric rhodamine–naphthalimide pH selective probe built on the basis of a PAMAM light-harvesting architecture. *J. Lumin.* **158**, 50–59.
9. Qiao, Z. and X. Shi (2015) Dendrimer-based molecular imaging contrast agents. *Prog. Polym. Sci.* **44**, 1–27.
10. Alamry, K. A., N. I. Georgiev, S. A. El-Daly, L. A. Taib and V. B. Bojinov (2015) A highly selective ratiometric fluorescent pH probe based on a PAMAM wavelength-shifting bichromophoric system. *Spectrochim. Acta A Mol. Biomol. Spectrosc.* **135**, 792–800.
11. Kaastrup, K. and H. D. Sikes (2015) Investigation of dendrimers functionalized with eosin as macrophotoinitiators for polymerization-based signal amplification reactions. *RSC Adv.* **5**, 15652–15659.
12. Karthikeyan, K., A. Babu, S.-J. Kim, R. Murugesan and K. Jeyasubramanian (2011) Enhanced photodynamic efficacy and efficient delivery of Rose Bengal using nanostructured poly(amidoamine) dendrimers: Potential application in photodynamic therapy of cancer. *Cancer Nanotechnol.* **2**, 95–103.
13. Tomalia, D. A., A. M. Naylor and W. A. Goddard (1990) Starburst dendrimers: Molecular-level control of size, shape, surface chemistry, topology, and flexibility from atoms to macroscopic matter. *Angew. Chem. Int. Ed. Engl.* **29**, 138–175.
14. Thota, B. N. S., L. H. Urner and R. Haag (2016) Supramolecular architectures of dendritic amphiphiles in water. *Chem. Rev.* **116**, 2079–2102.
15. Jansen, J. F. G. A., E. W. Meijer and E. M. M. De Brabander - Van Den Berg (1996) Bengal rose@ dendritic box. *Macromol. Symp.* **102**, 27–33.
16. Balzani, V., P. Ceroni, S. Gestermann, M. Gorka, C. Kauffmann, M. Maestri and F. Vogtle (2000) Eosin molecules hosted into a dendrimer which carries thirty-two dansyl units in the periphery: A photophysical study. *ChemPhysChem* **1**, 224–227.
17. Balzani, V., P. Ceroni, S. Gestermann, M. Gorka, C. Kauffmann and F. Vögtle (2002) Fluorescent guests hosted in fluorescent dendrimers. *Tetrahedron* **58**, 629–637.
18. Aumanen, J., V. Lehtovuori, N. Werner, G. Richardt, J. van Heyst, F. Vögtle and J. Korppi-Tommola (2006) Ultrafast energy transfer in dansylated POPAM–eosin complexes. *Chem. Phys. Lett.* **433**, 75–79.
19. Aumanen, J., T. Kesti, V. Sundstrom, G. Teobaldi, F. Zerbetto, N. Werner, G. Richardt, J. van Heyst, F. Vogtle and J. Korppi-Tommola (2010) Internal dynamics and energy transfer in dansylated POPAM dendrimers and their eosin complexes. *J. Phys. Chem. B* **114**, 1548–1558.
20. Aumanen, J., G. Teobaldi, F. Zerbetto and J. Korppi-Tommola (2011) The effect of temperature on the internal dynamics of dansylated POPAM dendrimers. *RSC Adv.* **1**, 1778–1787.
21. Aumanen, J. and J. Korppi-Tommola (2011) Energy transfer to xanthene dyes in dansylated POPAM dendrimers. *Chem. Phys. Lett.* **518**, 87–92.
22. Dougherty, C. A., J. C. Furgal, M. A. van Dongen, T. 3rd Goodson, M. M. Banaszak Holl, J. Manono and S. DiMaggio (2014) Isolation and characterization of precise dye/dendrimer ratios. *Chem. Eur. J.* **20**, 4638–4645.
23. Kline, K. K., E. J. Morgan, L. K. Norton and S. A. Tucker (2009) Encapsulation and quantification of multiple dye guests in unmodified poly(amidoamine) dendrimers as a function of generation. *Talanta* **78**, 1489–1491.
24. Morgan, E. J., J. M. Rippey and S. A. Tucker (2006) Spectroscopic characterization of poly(amidoamine) dendrimers as selective uptake devices: Phenol blue versus Nile red. *Appl. Spectrosc.* **60**, 551–559.
25. Arbeloa, E. M., C. M. Previtali and S. G. Bertolotti (2016) Study of the Eosin-Y/PAMAM interactions in alkaline aqueous solution. *J. Lumin.* **172**, 92–98.
26. Arbeloa, E. M., C. M. Previtali and S. G. Bertolotti (2016) Photochemical study of Eosin-Y with PAMAM dendrimers in aqueous solution. *J. Lumin.* **180**, 369–375.
27. Arbeloa, E. M., C. M. Previtali and S. G. Bertolotti (2018) A comparative study on the photophysics and photochemistry of xanthene dyes in the presence of polyamidoamine (PAMAM) dendrimers. *ChemPhysChem* **19**, 934–942.
28. Suchetti, C. A., A. I. Novaira, S. G. Bertolotti and C. M. Previtali (2009) The excited states interaction of safranine-O with PAMAM and DAB dendrimers in methanol. *J. Photochem. Photobiol. A Chem.* **201**, 69–74.
29. Militello, M. P., M. Altamirano, S. G. Bertolotti and C. M. Previtali (2018) The excited states interaction of safranine-O with low generation carboxyl terminated PAMAM dendrimers in aqueous medium. *Photochem. Photobiol. Sci.* **17**(5), 652–659.
30. Abderrezak, A., P. Bourassa, J.-S. Mandeville, R. Sedaghat-Herati and H.-A. Tajmir- Riahi (2012) Dendrimers bind antioxidant polyphenols and cisPlatin drug. *PLoS ONE* **7**, e33102.
31. Hansen, J. S., M. Ficker, J. F. Petersen, B. E. Nielsen, S. Gohar and J. B. Christensen (2013) Study of the complexation of oxacillin in 1-(4-carbomethoxypyrrolidone)-terminated PAMAM dendrimers. *J. Phys. Chem. B* **117**, 14865–14874.
32. van de Weert, M. and L. Stella (2011) Fluorescence quenching and ligand binding: A critical discussion of a popular methodology. *J. Mol. Struct.* **998**, 144–150.
33. Ahumada, M., E. Lissi, A. M. Montagut, F. Valenzuela-Henríquez, N. L. Pacioni and E. I. Alarcon (2017) Association models for binding of molecules to Nanostructures. *Analyst* **142**, 2067–2089.
34. Altamirano, M. S., M. E. Grassano, S. G. Bertolotti and C. M. Previtali (2016) Photophysics and photochemistry of mercurochrome in reverse micelles. *J. Photochem. Photobiol. A Chem.* **329**, 149–154.
35. Gómez, M. L., C. M. Previtali and H. A. Montejano (2004) Photophysical properties of safranine-O in protic solvents. *Spectrochim. Acta A Mol. Biomol. Spectrosc.* **60**, 2433–2439.
36. Cakara, D., J. Kleimann and M. Borkovec (2003) Microscopic protonation equilibria of Poly(amidoamine) dendrimers from macroscopic titrations. *Macromolecules* **36**, 4201–4207.

37. Niu, Y., L. Sun and R. M. Crooks (2003) Determination of the intrinsic proton binding constants for poly(amidoamine) dendrimers via potentiometric pH titration. *Macromolecules* **36**, 5725–5731.
38. Sánchez-Barragán, I., J. M. Costa-Fernández and A. Sanz-Medel (2005) Tailoring the pH response range of fluorescent-based pH sensing phases by sol–gel surfactants co-immobilization. *Sens. Actuators, B* **107**, 69–76.
39. Fleming, G. R., A. W. E. Knight, J. M. Morris, R. J. S. Morrison and G. W. Robinson (1977) Picosecond fluorescence studies of xanthene dyes. *J. Am. Chem. Soc.* **99**(13), 4306–4311.
40. Chrysochoos, J., J. Ovadia and L. I. Grossweiner (1967) Pulse radiolysis of aqueous Eosin. *J. Phys. Chem.* **71**, 1629–1636.
41. Tachikawa, T., Y. Kobori, K. Akiyama, A. Katsuki, U. E. Steiner and S. Tero-Kubota (2002) Spin dynamics and zero-field splitting constants of the triplet exciplex generated by photoinduced electron transfer reaction between erythrosin B and duroquinone. *Chem. Phys. Lett.* **360**, 13–21.
42. Encinas, M. V., A. M. Rufs, S. G. Bertolotti and C. M. Previtali (2009) Xanthene dyes/amine as photoinitiators of radical polymerization: A comparative and photochemical study in aqueous medium. *Polymer* **50**, 2762–2767.
43. Baumgartnher, C. E., H. Richtol and D. A. Aikens (1981) Transient photochemistry of safranin-O. *Photochem. Photobiol.* **34**, 17–22.
44. Borsarelli, C. D., S. G. Bertolotti and C. M. Previtali (2002) Thermodynamic changes in the photoinduced proton-transfer reaction of the triplet state of safranine-T. *Photochem. Photobiol. Sci.* **1**, 574–580.
45. Arbeloa, E. M., G. V. Porcal, S. G. Bertolotti and C. M. Previtali (2013) Effect of the interface on the photophysics of eosin-Y in reverse miceles. *J. Photochem. Photobiol. A Chem.* **252**, 31–36.
46. Guha, S. N. and J. P. Mittal (1997) Pulse radiolysis study of one-electron reduction of safranine T. *J. Chem. Soc., Faraday Trans.* **93**, 3647–3652.